IEEE Photonics Journal
An IEEE Photonics Society Publication

Open Access

Low-Loss Buried-Heterostructure Optical Waveguide Based on Impurity-Free-Vacancy-Diffusion Quantum Well Intermixing

Volume 12, Number 2, April 2020

Yang-Jeng Chen
Rih-You Chen
Chih-Hsien Chen
Yu-Hung Lin
Cong-Long Chen
Po-Yun Wang
Yen-Hsiang Chang
Yi-Jen Chiu

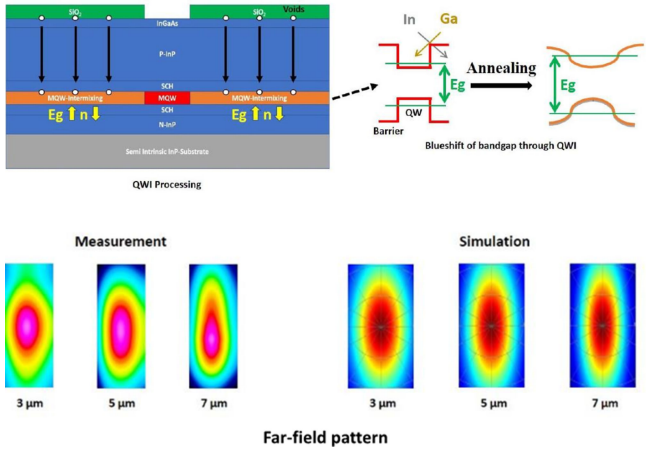

DOI: 10.1109/JPHOT.2020.2978401

Low-Loss Buried-Heterostructure Optical Waveguide Based on Impurity-Free-Vacancy-Diffusion Quantum Well Intermixing

Yang-Jeng Chen, Rih-You Chen, Chih-Hsien Chen, Yu-Hung Lin, Cong-Long Chen, Po-Yun Wang, Yen-Hsiang Chang, and Yi-Jen Chiu

Institute of Electro-Optical Engineering and Department of Photonics, National Sun Yat-sen University, Kaohsiung 804, Taiwan

DOI:10.1109/JPHOT.2020.2978401

Manuscript received December 12, 2019; revised February 3, 2020; accepted February 28, 2020. Date of publication March 4, 2020; date of current version March 23, 2020. This work was supported by the Ministry of Science and Technology, Taiwan (MOST 105-2221-E-110-043- and MOST 108-2218-E-110-011). Corresponding author: Yi-Jen Chiu (e-mail: yjchiu@faculty.nsysu.edu.tw).

Abstract: A new method for fabricating a high-quality buried-heterostructure optical waveguide using quantum well intermixing (QWI) has been demonstrated. By patterning a SiO_2 thin film on top of a multiple quantum well (MQW) heterostructure, rapid thermal annealing (RTA) could induce laterally local QWI, resulting in a bandgap blueshift and a simultaneous decrease in the refractive index. Both lateral bandgap and index engineering could be attained along the MQW plane, which could be used for a buried-heterostructure optical waveguide. Two SiO_2 strips with 3, 5 and 7 μm windows were fabricated for waveguide on a 1540 nm InGaAsP MQW sample. A 120 nm blueshift under the SiO_2 area was observed, leading to the index contrast of 0.07. Far-field optical diffraction measurements were also performed to yield angles of 13.9°, 12.8° and 10.6°. A narrower window resulted in a narrower optical waveguide width and exhibited a larger diffraction angle, suggesting that QWI defined the buried optical waveguide. In addition, an electroabsorption modulator was also made by buried waveguide. A -10 dB low optical insertion loss and a 15 dB high extinction ratio in a 500 μm long waveguide were obtained, indicating that a buried heterostructure could be used for photonic devices and integration applications.

Index Terms: Quantum well intermixing, low loss waveguide, buried waveguide, electroabsorption modulator (EAM).

1. Introduction

Optical waveguide technology that uses III–V semiconductor materials plays an important role in photonic integrated circuits because the integrated performance of the devices or modules relies primarily on the waveguide properties. The ultralow loss of the optical waveguide is needed in passive elements to convey optical signals without loss or to perform optical field interference to achieve the desired functions, such as those of a filter and a wavelength division multiplexer (WDM). On the other hand, high-performance active waveguides need high optical and carrier confinement factors to exhibit high-efficient active properties, such as those of a laser, modulator and detector.

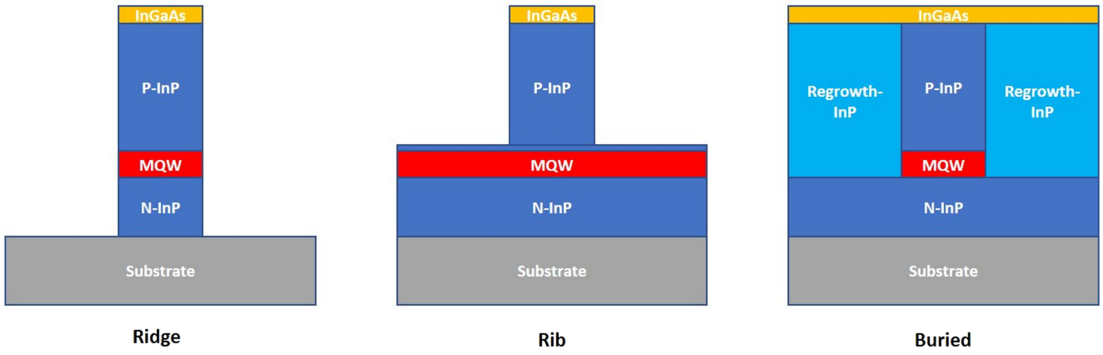

Fig. 1. The schematic diagrams of waveguide structure made by III–V semiconductor.

Only several parameters are necessary to enhance device performance, such as waveguide loss and optical and carrier confinement.

Several types of optical waveguide technologies, such as ridge waveguide, rib waveguide and buried heterostructure waveguide [1], have been developed. Fig. 1 shows a schematic diagram of the optical waveguide structure that is made with an III–V semiconductor material. The ridge structure of the waveguide was defined by etching through the active region to form sidewall interfaces. Thus, the high-index contrast between the active region and the surrounding material leads to high optical confinement and low junction capacitance. In addition, the high quality passivation on the etching surface needs to be made to reduce the leakage current [2]. Another approach that is similar to the ridge waveguide is the rib waveguide structure. The etching depth was made to stop near the top of the active region through the selective etching scheme [3]. Thus, the leakage current can be reduced. However, the optical mode will be extended along the horizontal directions, which lowers the optical and current confinement. Therefore, the waveguide structure fabricated by burying the active region in a higher bandgap material is one of the best schemes. By suitably defining the types of doping in the surrounding material for electrical barrier, high quality electrical confinement with good optical mode and low leakage current can be achieved, leading to the high performance of active devices [4].

Typically, buried waveguides are fabricated by the epi-layer with successive regrowth steps. The material with a higher bandgap and lower refractive index will cover and fill the sidewalls of the waveguide after etching the active region, which will form the lateral and vertical heterostructure. However, this fabrication scheme has technological challenges, such as (1) the passivation to remove the defects or vacancies and (2) the smooth surface on the junctions between two cladding layers and the surrounding region of the patterned active region. The doping diffusion in the regrown epi-layers will change the doping level of the designed layer structure, which will result in a different performance in the active region. Due to the abovementioned technological challenges, the development of the buried waveguide using simple, cost-effective schemes to improve the reliability of fabrication is one of the technologies for the future photonic integration.

Consequently, we developed a new technique for buried waveguide fabrication using impurity free vacancy disorder (IFVD) QWI. IFVD QWI is a bandgap engineering approach. By depositing the capping layers (e.g., SiO_2 or Si_3N_4) on the top layers followed by the subsequent RTA, the vacancies are generated and diffuse into the MQW, which enhances the intermixing of atoms during thermal annealing. Because of the intermixing between quantum wells and barriers, the effective bandgap blueshifts to the shorter optical wavelength, and the refractive index changes due to the Kramers-Kronig relation [5]. Thus, the higher the bandgap is optimized, and the lower is refractive index is formed. Therefore, using QWI, the bandgap can be controlled, and the corresponding refractive index can be engineered. Thus, using the patterned capping layer, local QWI can induce the buried heterostructure (in the plane of MQW) and, simultaneously, the refractive-index difference with the other area (non-QWI area). Through the patterned strip size of local QWI, the

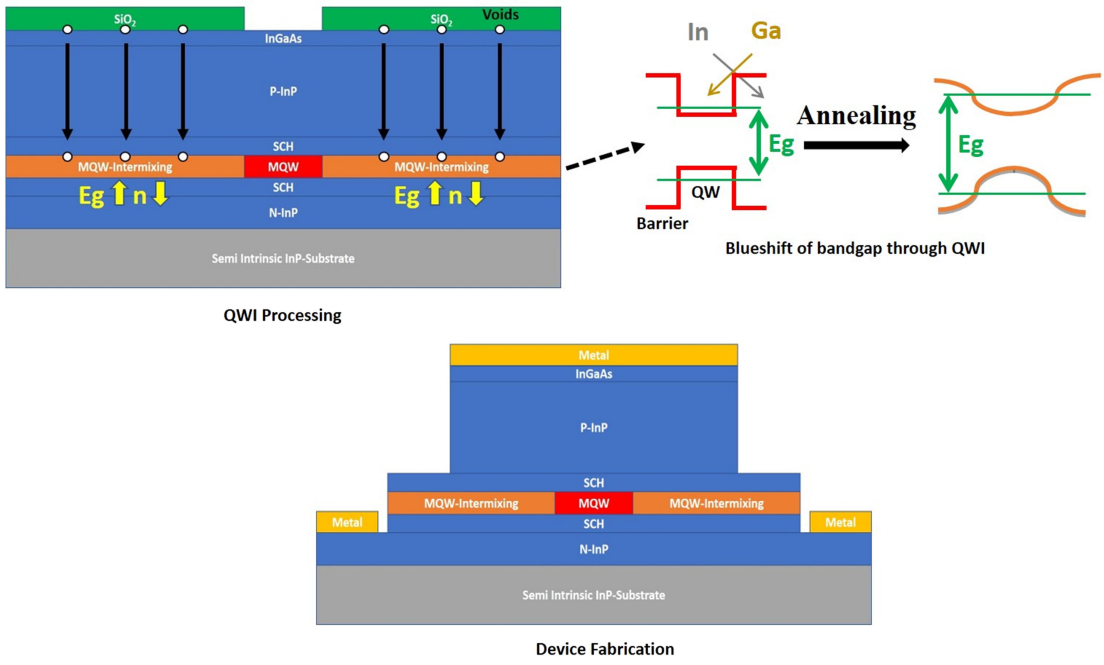

Fig. 2. Schematic diagrams of the material layer structure (top left), the QWI process (top left), the bandgap blueshift due to QWI (top right), and the definition of buried waveguide using QWI (bottom). The MQW is based on the InGaAsP-based material. Through IFVD processing, the area for QWI locally induces a higher refractive index from the blueshift of the bandgap in MQW.

buried type of optical waveguide fabrication can be expected. In addition, due to the blueshift of the bandgap, the carrier confinement can result in an efficient active performance.

In this paper, using efficient local IFVD QWI processing on an InGaAsP-based MQW heterostructure, we demonstrate the processing of a buried-type optical waveguide. During the process, no epi-layer regrowth was used. By patterning the SiO_2 capping layer with different widths of strip structures, the buried optical waveguide fabrication was demonstrated. By measuring the far-field patterns of the optical waveguide, the refractive index confinement was confirmed, which was consistent with the simulation results. In addition, the electro-absorption modulator was defined through IFVD QWI [6]. The strong Fabry-Perot oscillation and quantum confined Stark effect were observed, which suggested that the low optical loss and carrier confinement were achieved using this kind of buried waveguide.

2. Optical Waveguide Design, QWI Processing and Fabrication

To design the heterostructure of the buried optical waveguide using QWI, the optical mode distribution of this optical waveguide is first simulated before performing QWI processing. Mode solution software (Lumerical) was used as the simulation tool. Fig. 2 shows the schematic diagram of the layer structure and the local QWI processing to define the buried heterostructure of the buried optical waveguide. A 1550 nm InGaAsP-based MQW was used as the material in QWI intermixing, where the overall designed material structure was set as the p-i-n junction (MQW is in the i-layer). The P-type and N-type doped InP-layer was used for the top and bottom cladding layers, respectively. By defining the open window of the SiO_2 capping layer on top of the material, the buried waveguide structure could be set after the QWI intermixing, where the open window defined the area of the optical waveguide, i.e., after the QWI of the refractive index under the SiO_2 capping layer reduced from the blueshift of the bandgap. In the simulation, a 3 μm width of the open window was used. To further examine the QWI-induced refractive index change, the

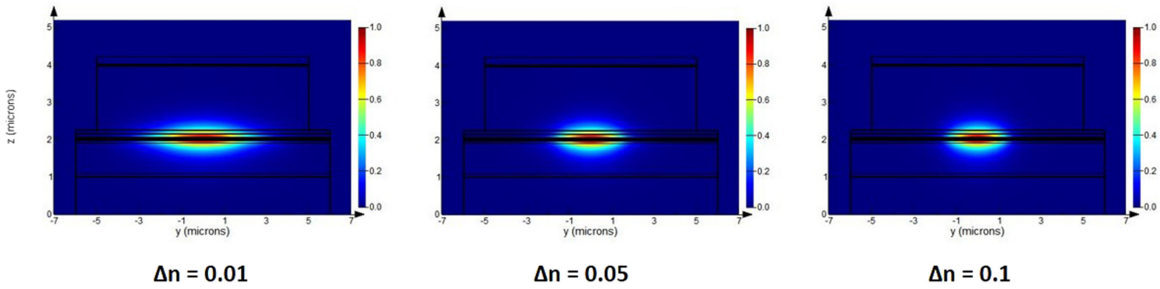

Fig. 3. Simulated optical mode profile at 3 μm width of buried waveguide, where the refractive index contrasts are 0.01, 0.05, and 0.1.

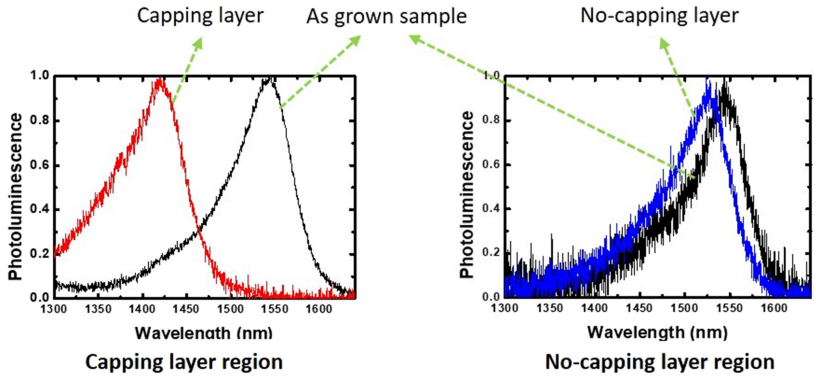

Fig. 4. PL spectra of the buried waveguide by comparing with as-grown sample, where the capping layer (left) and the no-capping layer (right) were measured.

index contrast between the open window and capping-layer region was calculated to simulate the optical mode properties. As shown, with QWI in the InGaAsP material, the interdiffusion of atoms inside the MQW redistributes the composition of atoms, which increases the bandgap of MQW. The bandgap can be calculated based on the physical model in [5]. To further simulate the corresponding refractive index of MQW, the Kramers-Kronig (K-K) relation was used to calculate the refractive index in the QWI region [7], where the dispersion relation of the optical absorption change was calculated based on the material composition in MQW. According to the K-K relation, the variation of the refractive index is related to the change in the bandgap absorption with the bandgap shift. Using this method, we consider the refractive index in the QWI region as a bulk and calculated it from the PL spectrum. After setting the structure model, the optical mode is simulated based on the refractive index contrast of 0.01, 0.05, and 0.1. Fig. 3 shows the optical modes. The higher the index contrast is, the more confined the optical mode is. As the index contrast is larger than 0.05, optical modes are well confined within the set open window. Consequently, to design the high confinement of the optical mode within the experiment tolerance, the index contrast of 0.07 was used. The corresponding bandgap shift is 100 nm (0.057 eV).

During the device fabrication, the buried optical waveguide based on InGaAsP MQW was fabricated by the QWI method. A 200 nm thick SiO_2 was deposited as the capping layer on top of the wafer by an electron gun beam evaporator system. Fig. 2 shows that to further characterize the optical waveguide properties, three kinds of waveguide patterns with widths of 3 μm, 5 μm and 7 μm are defined by opening a widow on the SiO_2 film using photo lithography and SiO_2-etching. Based on the process described in a previous study [8], an H_2O_2 treatment under a CO_2 supercritical fluid was used to increase the oxygen content in SiO_2 to improve the QWI processing. The samples with a patterned SiO_2 capping layer were treated under RTA at 650 °C for 90 s. Fig. 4 shows the photoluminescence (PL) spectra measurements of MQW for the capping-

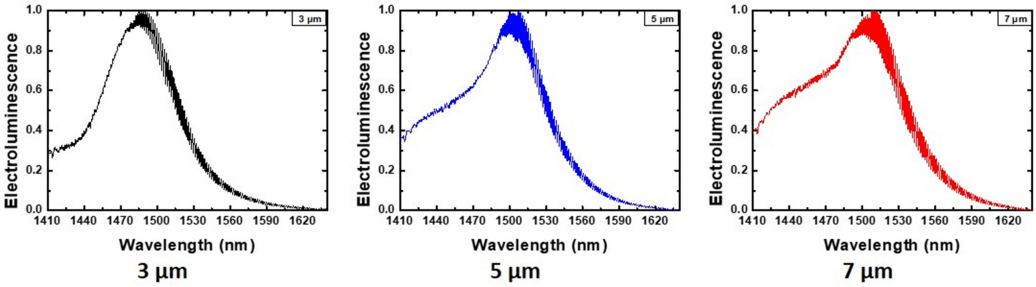

Fig. 5. EL spectra obtained by injecting current into the 3 μm, 5 μm, and 7 μm buried waveguide.

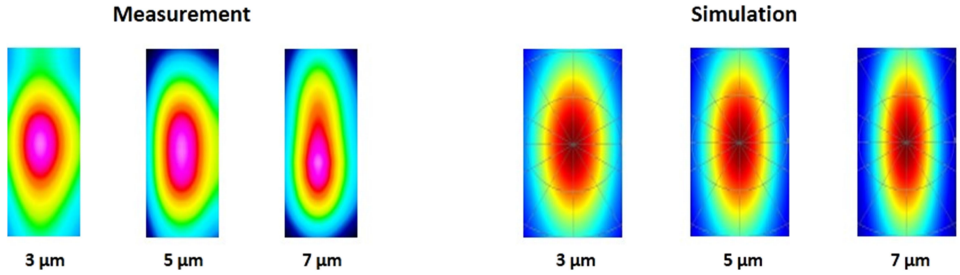

Fig. 6. Far-field measurements (left) and the simulation (right) for 3 μm, 5 μm, and 7 μm buried waveguides via optical transmission.

and no-capping layer regions; the capping-layer region shows a large blue shift due to the capping layer from 1540 nm to 1420 nm. No significant shift in the MQW region without a capping layer was observed compared to the as-grown sample, which suggests that capping can effectively lead to bandgap engineering. Because the substrate is semi-insulating InP, a 10 μm wide mesa was defined by etching through the MQW layers for n-contact metallization and covered the buried waveguide regions. Ti/Pt/Au and Ni/AuGe/Ni/Au were deposited to achieve P-type and N-type ohmic contact metallization, respectively. A bisbenzocyclotene (BCB) material was spun to cover the whole mesa, which passivated the etching surface and achieved planarization. Finally, Ti/Au was deposited to create a coplanar-waveguide (CPW) electrical wire to produce an electrical feed line.

3. Optical Measurement and Waveguide Characterization

After performing the local QWI on both sides of the open window to enlarge the energy bandgap, the carriers inside the window experience electrical confinement. Thus, an efficient optical emission by current injection can be created. To examine the effects on the electrical confinement, electro-luminance (EL) by current injection in the p-i-n junction on the samples was first performed to examine the active region of the waveguide after QWI. Fig. 5 shows the EL spectra obtained by forward biasing the diodes for three buried waveguide (open window) conditions. Clearly, the EL peaks at 1495 nm, 1505 nm and 1510 nm were observed for the 3 μm, 5 μm and 7 μm buried waveguides. In comparison to the PL spectrum, the peaks at 1400 nm for the capping SiO_2 region (QWI region) and 1520 nm for the no-capping region are observed. Therefore, EL is mainly attributed to light generation from the MQW between the capping regions, which confirms that the strong electrical confinement can be achieved using this process.

To further test the optical wave propagation in the buried QWI-defined heterostructure, the optical field transmission and the related mode field patterns were characterized. Due to the local QWI, the energy-level difference of MQW induces the index contrast, which allows to fabricate an optical waveguide. By measuring the optical transmission and the output mode field pattern of the

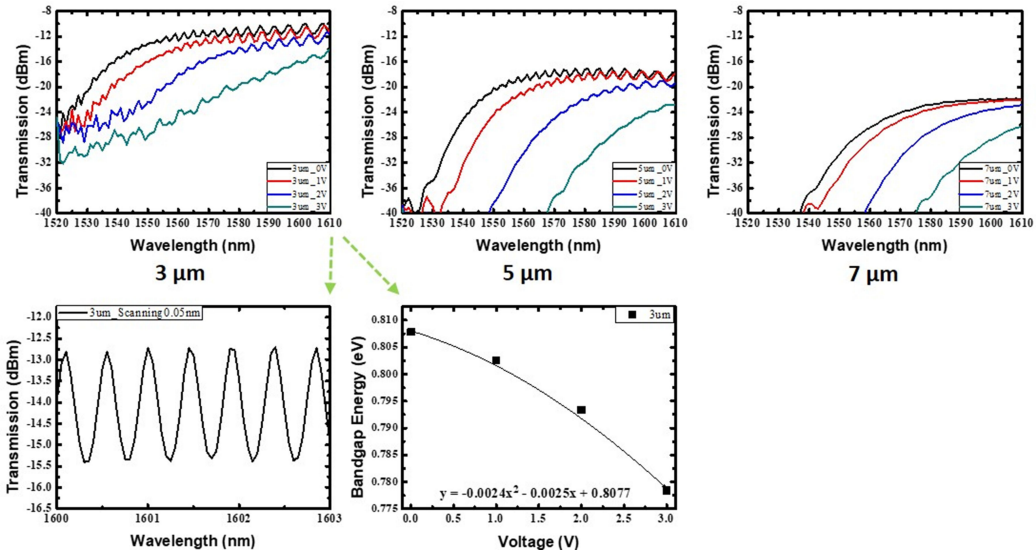

Fig. 7. (Top) the measured optical transmission spectra of the waveguide for different bias values. (Bottom) the measured Fabry-Perot oscillation of optical transmission for 3 μm buried waveguide near 1600 nm wavelength and the extracted bandgap edge of MQW versus the bias. The quadratic relation indicates the QCSE of the buried MQW.

waveguide, the optical waveguide properties can be extracted with comparing to the simulation results. Because the EL spectrum is almost below 1540 nm, a 1550 nm light near the band edge was injected by a tunable laser into the buried heterostructure for the optical transmission measurement of the waveguide and to test the quantum confined Stark effect of the waveguide. The input light was coupled by a tapered fiber, and far-field patterns were measured at the output of the waveguide. Fig. 6 shows the measured far-field patterns. By measuring the buried waveguides using the 3 μm, 5 μm and 7 μm width of the open window, the optical refraction angles of 13.9, 12.8, and 10.6°, respectively, were extracted in the horizontal direction (parallel to the MQW plane), and optical refraction angles of 27.8, 29.2, and 30.1°, respectively, were extracted in the vertical direction. Because the same MQW was used in all devices, almost the same far-field angle in the vertical direction was observed. In addition, the larger open widow of QWI is, the smaller angle is in the horizontal direction, suggesting that the size of the buried QWI-defined heterostructure governs the field diffraction. To investigate this behavior, the change in the bandgap from the QWI processing was used to extract the index contrast based on the K-K relation [5]. Then, the diffraction patterns were calculated for comparison with the measurement. The simulated far-field refraction angles are 11.6, 10.5 and 8° in the horizontal direction (parallel to the MQW plane), and 29.5, 29.6 and 29.5° in the vertical direction. These results are consistent with the measurement, which confirms that the buried heterostructure defined by the local QWI is able to form the optical confinement for the optical waveguide application.

The optical loss in the waveguide and the optical mode confinement in the active region are important parameters for the performance of the active optical waveguide. To examine the effects of the QWI processing on the buried waveguide, the Fabry-Perot (FP) resonant cavity behavior was measured to extract the optical loss. The quantum confined Stark effect (QCSE) against with the reversed bias of the p-i-n junction was also measured to investigate the electro-absorption behavior in the buried MQW region. The 500 μm waveguide length with the 3 μm, 5 μm and 7 μm open window on the capping layer was fabricated. In addition, no coating was used for the two facets of the waveguide. Thus, the interface of waveguide facets with air forms the FP optical resonator. The measured optical transmission spectra against with different reversed biases (e.g., 0, 1, 2 and 3 V) of the p-i-n junction are shown in the top of Fig. 7, where the input laser light spectra were obtained from 1520 nm to 1610 nm. Clearly, in the short wavelength regime or at high bias (especially at

3 V), no significant FP oscillations are observed due to the high intrinsic optical absorption in MQW. Nevertheless, stronger FP oscillations occur by increasing the optical wavelengths, which suggests that the optical propagation loss inside the waveguide is considerably reduced. By selecting the wavelength regime of 1600 nm (long wavelength) and a low bias condition, the loss of 10 dB and the extinction ratio of 15 dB are observed, which results from the waveguide scattering due to QWI processing. As shown in the bottom of Fig. 7, the measured FP oscillation (from 1600 nm to 1603 nm) was plotted. The corresponding optical transmission loss is 9.59 (cm^{-1}). The low waveguide insertion loss of 10 dB was measured from the long wavelength regime, which includes the reflection loss at facet mirror, fiber coupling loss, and waveguide propagation loss. The low propagation loss is mainly attributed to the buried optical waveguide structure through QWI processing. Moreover, by extracting the value of the MQW bandgap edge against the bias, the bottom of Fig. 7 shows a clearly quadratic relation, which further confirms the QCSE of the MQW in the buried heterostructure.

4. Conclusion

In this paper, we demonstrated a novel method for fabricating a low loss buried-heterostructure waveguide by IFVD QWI. By depositing and patterning the SiO_2 capping layer, three open windows are defined (e.g., 3 μm, 5 μm and 7 μm), and a 110 nm large blueshift was obtained after 90 s of RTA processing at 650 °C, which resulted in a 0.07 refractive index contrast. The far field mode measurement is consistent with the simulation result, which shows the smaller diffraction angle with a wider window in the horizontal direction. The peak of the EL spectrum (approximately 1510 nm) is near the bandgap of the no-capping layer (1520 nm), which indicates that the carriers are mainly confined and recombine in the no-capping region. In addition, this buried waveguide was tested as the EA modulator with a reverse bias, and a 15 dB extinction ratio was extracted, which confirmed the strong QCSE. A strong Fabry-Perot oscillation was observed at 1600 nm, which suggests that the optical loss is reduced in this buried waveguide. Consequently, this novel buried waveguide with the electrical and optical confinement can be applied to high performance photonic devices.

Acknowledgment

The authors would like to thank the financial supports from the Ministry of Science and Technology, Taiwan (MOST 105-2221-E-110-043- and MOST 108-2218-E-110-011). Also, the authors would like to thank the wafer growth from Land Mark Optoelectronic Corporation.

References

[1] K. Okamoto, *Fundamentals of Optical Waveguides*, 2nd ed. Cambridge, Massachusetts, USA: Academic press, 2006.
[2] K. Nakahara *et al.*, "40-Gb/s direct modulation with high extinction ratio operation of 1.3-μm InGaAlAs multiquantum well ridge waveguide distributed feedback lasers," *IEEE Photon. Technol. Lett.*, vol. 19, no. 19, pp. 1436–1438, Oct. 2007.
[3] R. J. Deri and E. Kapon, "Low-loss III–V semiconductor optical waveguides," *IEEE J. Quantum Electron.*, vol. 27, no. 3, pp. 626–640, Mar. 1991.
[4] A. Evans, S. R. Darvish, S. Slivken, J. Nguyen, Y. Bai, and M. Razeghi, "Buried heterostructure quantum cascade lasers with high continuous-wave wall plug efficiency," *Appl. Phys. Lett.*, vol. 91, no. 7, 2007, Art. no. 071101.
[5] S. Adachi, "Optical dispersion relations for GaP, GaAs, GaSb, InP, InAs, InSb, AlxGa1−xAs, and In1−xGaxAsyP1−y," *J. Appl. Phys.*, vol. 66, no. 12, pp. 6030–6040, 1989.
[6] C. H. Chen, P. Y. Wang, R. Y. Chen, C. L. Chen, Y. J. Chen, and Y. J. Chiu, "Local quantum well intermixing, for fabricating high-speed electroabsorption modulator," in *Proc. IEEE Photon. Conf.*, 2018, pp. 1–2.
[7] B. S. Ooi *et al.*, "Selective quantum-well intermixing in GaAs-AlGaAs structures using impurity-free vacancy diffusion," *IEEE J. Quantum Electron.*, vol. 33, no. 10, pp. 1784–1793, Oct. 1997.
[8] Y. J. Chen *et al.*, "Supercritical fluid-enhanced IFVD quantum well intermixing for the regrowth-free photonic integration of EAM and SOA," *Opt. Mater. Express*, vol. 8, no. 9, pp. 2592–2599, 2018.